Ice/rock porous mixtures: compaction experiments and interpretation

J. LELIWA-KOPYSTYŃSKI

Institute of Geophysics, University of Warsaw, Pasteura 7, 00-093 Warszawa, Poland

N. MAENO

Institute of Low Temperature Science, Hokkaido University, Sapporo 060, Japan

ABSTRACT. Compaction experiments on porous samples of granular ice and ice/rock mixtures were conducted at low temperature, primarily to obtain rheological data useful in modeling the internal structure and evolution of icy satellites of the giant planets. The data may also be of interest for studying Earth's glaciers and the Martian polar caps.

The samples tested were prepared from three types of ice: water, carbon dioxide and ammonia; three types of rock components were also used in the samples. The time-dependent compaction of samples a few centimeters in size was studied for a range of rock contents, pressures (2.2–17.7 MPa) and temperatures (140–261 K). An equation (16), giving the compaction rate as a function of porosity, pressure, temperature and concentration of the rock component was fitted to the observed results. The presence of rock fragments strongly inhibits the compaction process.

LIST OF SYMBOLS, ABBREVIATIONS AND NUMERICAL CONSTANTS

C_m	Concentration by mass of rock component
C_v	Concentration by volume of rock component
m	Total sample mass (g)
m_i	Mass of ice in a sample (g)
m_r	Mass of rock in a sample (g)
p	Pressure (MPa)
q	Porosity: (volume of voids)/(volume of sample)
r_i	Mean radius of ice grains (cm)
r_r	Mean radius of rock grains (cm)
T	Temperature (K)
$\dot{\epsilon}$	Densification rate (s^{-1})
ρ	Density (Mg m^{-3})
H$_2$O	Water ice or snow
gn.-lhz.	Garnet-lherzolite
met.	Stony meteorite
snd.	Sandstone

Bulk densities, in Mg m^{-3}, used in numerical calculations:

$\rho_i = 0.918$	Water ice, H$_2$O
$\rho_i = 0.9$	Ammonia ice, (NH$_3$)$_x$(H$_2$O)$_{1-x}$ where $x = 0.25$--0.28
$\rho_i = 1.56$	Carbon dioxide, CO$_2$
$\rho_r = 3.06$	Garnet-lherzolite
$\rho_r = 2.54$	Sandstone
$p_r = 3.41$	Stony meteorite, Ym 74013

The experimental data are labeled by the run number as follows:

(i) Numbers refer to experiments with pressure produced by loading a piston with weights.
(ii) Numbers followed by M refer to experiments with hydraulic press apparatus.

1. INTRODUCTION

This experimental work originated from theoretical considerations that concern modeling of the internal structure of the icy satellites of giant planets (Eluszkiewicz and Leliwa-Kopystyński, 1988, 1989). Thanks to Voyager 1 and 2 space missions, the global physical parameters of these satellites (see Table 1) are quite well known at present. Astronomical, cosmochemical and spacecraft close-encounter data suggest that so-called "icy satellites" are composed mostly of water ice with some admixtures of other materials which could be rocks (silicates similar to those known on Earth(?), stony meteorite-type rocks(?)) and solidified gases such as ammonia, methane and others, commonly referred to as "ices". The proportion of the mass of a satellite that is composed of rock can easily be deduced from the known mean density of the satellite and the densities of water ice and other materials assumed to comprise the satellite. However, the C_m values listed in Table 1 are of dubious value in view of one important question: why should an

Table 1. Selected physical data for icy satellites

Satellite in order of size	Radius R^1	Mass M	Mean density ρ	Central pressure p^2	Rock content by mass C_m^3
	km	10^{20} kg	Mg m^{-3}	MPa	
U3 Titania	788.9 ± 1.8	34.8 ± 1.8	1.69 ± 0.09	249	0.60–0.69
U4 Oberon	761.4 ± 2.6	29.2 ± 1.6	1.58 ± 0.09	202	0.54–0.63
S5 Rhea	765 ± 5	24.9 ± 1.5	1.33 ± 0.09	144	0.35–0.49
S8 Iapetus	730 ± 10	18.8 ± 1.2	1.16 ± 0.09	99	0.18–0.36
U2 Umbriel	584.7 ± 2.8	12.7 ± 2.4	1.52 ± 0.29	110	0.34–0.70
U1 Ariel	578.9 ± 0.6	13.5 ± 2.4	1.66 ± 0.30	129	0.45–0.75
S4 Dione	560 ± 5	10.5 ± 0.3	1.43 ± 0.06	89	0.46–0.54
S3 Tethys	530 ± 10	7.55 ± 0.90	1.21 ± 0.16	58	0.15–0.46
S2 Enceladus	251 ± 5	0.84 ± 0.30	1.2 ± 0.4	14	0.00–0.60
U5 Miranda	235.8 ± 0.7	0.749 ± 0.224	1.36 ± 0.41	14	0.01–0.68
S1 Mimas	198.8 ± 0.6	0.375 ± 0.008	1.137 ± 0.018	7.1	0.23–0.27

Maximum pressures attained in our experiments, at −25°C: 17.6

at −195.8°C: 2.3

Rock-content range in our experiments: 0.0 –0.78

[1] Radii of Uranian satellites from Thomas (1986).

[2] Central pressure calculated from the formula for uniform self-gravitating body $p = 3GM^2/(4\pi R^4)$.

[3] C_m is the ratio (mass of rock)/(mass of satellite) calculated from the formula

$$C_m = \frac{\rho_r}{\rho} \frac{\rho - \rho_i}{\rho_r - \rho_i}$$

valid for a non-porous satellite.

icy satellite be a non-porous, fully compacted body? If it is porous, C_m is underdetermined. The compositional data (Table 1) become lower bounds of C_m.

Although this work is focused on applications related to the satellites, the rheological experiments on ice/rock samples may also be interesting in studying the dynamic behavior of other systems, including glaciers on Earth and the regolith and polar caps on Mars.

The experimental pressure range, up to 17.7 MPa, covers the whole interior of Mimas and Miranda, as well as the upper dozens of kilometers of other medium-sized icy satellites. Within the Martian crust and within Earth's glaciers the maximum pressure in our experiments corresponds to a depth of about 2 km.

Temperature and pressure regimes in the interior of the icy satellites do not preclude the possibility that the constituent material was porous at the time of satellite formation and has remained porous since. As Smoluchowski and others (1984) wrote "There is no reason to suppose that ices in the solar system whether on satellites, in cometary nuclei, on interplanetary grains or on the ring particles of Saturn have no pores". This opinion was recently proved for a cometary nucleus (Vega and Giotto missions revealed the density of the nucleus of Halley's comet to be 0.4–0.6 Mg m^{-3}), as well as for icy satellites (based on calculation of thickness of the regolith layer on

Mimas by Eluszkiewicz (1990)). In the initial efforts of modeling the porous structure of icy satellites, the porosity versus pressure relation was assumed ad hoc as being an exponential one and the material rheology was not considered (Eluszkiewicz and Leliwa-Kopystyński, 1988, 1989). In the most recent work (Eluszkiewicz, 1990), a model including the rheology of a one-component granular material (Ashby, 1988) was developed and applied to the modeling of the structure of Mimas and its evolution. In this model, however, the rheology of ice grains but not an ice/rock grain mixture was considered.

The experiments were performed at higher temperatures than those of icy satellites (surface temperatures of Saturnian and Uranian satellites are about 80 K and 60 K, respectively). However, temperatures higher than the current mean were attained during the formation of the satellites from dusty/grainy nebula composed of ices and minerals (Ellsworth and Schubert, 1983; Squyres and others, 1988). Moreover, diurnal temperature variations are considerable. For example, at the Viking landing sites on Mars, temperatures vary diurnally between about 190 and 240 K (Lewis and Prinn, 1984).

To improve modeling of the porous ice/rock structure of satellites, it is imperative to carry out rheological experiments on ice/rock mixtures at pressures and temperatures as close as possible to those expected in

the interior of satellites. Extrapolation of experimental results from laboratory temperatures to the lower temperatures of real satellites and from laboratory pressures, which do not cover the whole intervals of pressures expected in the satellites, may be necessary. Such an extrapolation should be done with caution, since the laboratory time-scale (days) differs from the time-scale of evolution (about 10^3–10^9 years) by 5–11 orders of magnitude. Results from experiments, which are conducted for practical reasons at elevated pressure and temperature, must then be extrapolated to the expected natural, p, T conditions. One can introduce the newly found rheological relations to the system of equations describing the structure of a satellite and seek to answer the question: "How did the porosity and other parameters describing a satellite's structure evolve from the satellite's initiation through a primitive post-accretional stage (when it had already reached its present mass) to the evolved present stage?"

Let us consider a two-component perfectly mixed granular body. It could be, for example, a centimeter-size laboratory sample, or a domain of a satellite sufficiently large to be considered a continuum, but sufficiently small for the pressure and temperature to be essentially uniform throughout the domain. Let one component be an ice with density ρ_i and the second one a rock with density ρ_r; their masses are m_i and m_r, respectively. The volume under consideration comprises

$$V_{\text{total}} = V_{\text{ice}} + V_{\text{rock}} + V_{\text{voids}}. \tag{1}$$

Under pressure it decreases with time mainly due to contracting voids and, to a much smaller extent, due to compaction of ice and rock (this part will be neglected from here on). The porosity q is defined as follows:

$$V_{\text{voids}} = qV_{\text{total}}. \tag{2}$$

The rock concentration by mass C_m and by volume C_v are

$$C_m = \frac{m_r}{m_i + m_r}, \quad C_v = \frac{V_r}{V_i + V_r}, \tag{3}$$

respectively. Therefore,

$$C_v = \frac{\rho_i C_m}{\rho_i C_m + \rho_r (1 - C_m)}, \quad \begin{array}{c} 0 < C_v < C_m \\ \text{for } \rho_r > \rho_i. \end{array} \tag{4}$$

The mean density of a body is

$$\rho = \frac{m_i + m_r}{V_{\text{total}}} = \rho_0 (1 - q) \tag{5}$$

where

$$\rho_0 = \frac{\rho_i \rho_r}{\rho_r (1 - C_m) + \rho_i C_m} \tag{6}$$

is the bulk density of a non-porous body.

In the following we will assume that the densities ρ_i and ρ_r are independent of pressure and temperature. The first assumption is physically reasonable for pressures applied in the experiments (up to 17.7 MPa), as well as for the pressures expected in medium-sized icy satellites (10 MPa and 150 MPa in the deep interiors of Mimas and Rhea, respectively). Neglecting thermal expansion is justifiable when comparing thermally induced changes of sample size to those expected due to void closure. For the

icy satellites, the volumetric strain due to thermal expansion can be estimated to be order 0.01, reflecting the thermal expansion coefficient and the expected temperature variability ($10^{-4} \text{K}^{-1} \times 10^2 \text{K}$). This is much less than the volume changes resulting from the closure of voids for any loosely sedimented granular material whose initial porosity is as high as 0.4. The volume of a sample under pressure decreases only by means of re-arrangement, crushing and coagulation of grains. Situations where phase transition can occur are excluded.

It follows from Equation (5) with constant ρ_0 that the rate at which density increases $\dot{\rho}$ is proportional to the rate at which porosity decreases $-\dot{q}$:

$$\dot{\rho} = -\rho_0 \dot{q}. \tag{7}$$

Therefore, using Equations (5) and (7), the strain rate $\dot{\epsilon}$ of a sample can be expressed as

$$\dot{\epsilon} \equiv \frac{1}{\rho} \dot{\rho} = -\frac{1}{1 - q} \dot{q}. \tag{8}$$

For low porosity, $q \to 0$, is $\dot{\epsilon} \cong -\dot{q}$. For convenience, hereafter, $-\dot{q}$ is referred to as the compaction rate.

2. SAMPLE PREPARATION

The composition of samples used in the 70 runs are listed in Table 2. Twenty-five runs were performed on water-ice samples without rock because they are relatively simple to interpret and, yet, they provide an instructive comparison with experiments using ice/rock mixtures.

The rocky fraction of the samples was prepared at normal room temperature. The temperature at which the granular icy component was prepared varied according to its melting (or sublimation) point. Accurate measurements of the mass were critical in the experiments. However, in some cases, considerable loss of ice by sublimation occurred as the icy material was weighed or mixed with the rock fraction (e.g. when a sample contained powdered water ice or when it was prepared from solid CO_2). This loss of ice cannot be distinguished from a porosity decrease of about 0.01. Although this effect is negligible for highly porous samples, it renders the measurement of compaction rate for highly compacted samples difficult and, in some cases, impossible.

We now describe the preparation method of the different components of the samples. The water-ice component of the samples was prepared in a cold room at 263 K or less. The millimeter-sized grains were produced from distilled water droplets formed by means of a medical-type injector on a polished aluminum sheet. Once frozen, the hemispherical icy grains were easily removed from the aluminum surface by slightly bending the sheet. The required mass of ice (about 35 g for pure ice samples and less for ice/rock samples was weighed and the grains were counted. One sample typically contained about 1000 grains. The average mass and radius of one quasi-hemispherical grain were about 0.03 g and 0.25 cm, respectively. The production of powder-sized ice grains was simpler and faster: they were made from blocks of natural snow by grating and sieving. The fraction with radii $r_i < 0.0885$ mm was used in most of the experiments with powder samples. The sample material was weighed

Table 2. List of experiments

1 Run #	2 Sample material	3 m_i/m_r or m_i only g	4 C_m	5 r_i/r_r or r_i only cm	6 q_0/q_f	7 p MPa	8 T K	9 10^5 s	10 κ
1, n	H_2O	22.9	0	~0.3		2.25	262	0.039	
2	H_2O	33.5	0	$0.24 < r_i < 0.30$	0.3817/0.0733	2.25	262	0.177	
3	H_2O	35.7	0	~0.3	0.4115/0.0909	2.25	262	0.571	
4	H_2O	36.4	0	0.300	0.3835/0.0106	2.25	262	6.480	
5	H_2O/gn.-lhz.	16.0/58.8	0.786	0.333/0.243	0.4840/0.3256	2.25	262	1.642	0.031
6	H_2O/snd.	16.5/48.0	0.744	0.306/0.226	0.4989/0.2742	2.25	262	1.545	0.200
7, a	H_2O	38.1	0	0.319	0.4327/0.0821	2.25	262	0.814	
8, a	H_2O/gn.-lhz.	21.6/28.6	0.57	0.292/0.249	0.4590/0.1751	2.25	262	13.728	0.034
9, n, a	H_2O	27.5	0	0.288	0.4316/0.1226	2.25	262	0.816	
10	H_2O	35.1	0	0.273	0.3723/0.0584	2.26	77/262	0.110/3.216	
11	H_2O	35.5	0	0.265	0.3501/0.0886	2.26	77/262	0.100/3.453	
12, n	H_2O/gn.-lhz.	21.6/28.5	0.57	0.241/0.191	0.4151/0.1843	2.26	77/262	0.100/4.204	0.038
13	H_2O/gn.-lhz.	21.6/28.5	0.57	0.212/0.191	0.3961/0.1696	2.26	77/262	0.124/10.810	0.028
14	ammonia ice	41	0	~0.35	0.4039/0.0899	2.26	77/178	0.30/0.66	
15, a	H_2O	35.5	0	0.241	0.3728/0.1266	2.26	77/262	0.14/3.229	
16, a	H_2O/gn.-lhz.	21.6/28.6	0.57	0.210/0.190	0.4080/0.0930	2.26	77/262	0.12/12.736	0.013
17, a	H_2O	29.8	0	0.226	0.3750/0.1340	2.26	195/251	1.311/2.542	
18, a	H_2O/gn.-lhz.	21.6/28.6	0.57	0.216/0.187	0.3948/0.0412	2.26	195/262	0.535/3.295	0.008
19, a	H_2O	30.9	0	<0.00885	0.4864/0.2009	2.26	262	0.658	
20, a	H_2O	33.8	0	<0.00885	0.4671/0.1245	3.73	262	2.869	
21, a	H_2O/gn.-lhz.	24.0/24.0	0.50	<0.00885/0.001	0.5100/0.1367	3.73	262	5.672	
22, a	H_2O/gn.-lhz.	19.8/19.8	0.50	$0.00885 < r_i, r_r < 0.0175$	0.4888/0.1272	3.73	262	6.082	
23, a	H_2O/gn.-lhz.	30.0/10.0	0.25	<0.00885/0.001	0.4907/0.0581	3.73	262	11.832	
24, a	H_2O	42.0	0	$0.021 < r_i < 0.0295$	0.3792/0.1754	2.26	262	7.047	
25, n,a	H_2O/gn.-lhz.	13.8/13.8	0.50	<0.00885/0.001	0.4868/0.0234	7.34	262	3.535	
26, n,a	H_2O/gn.-lhz.	15.0/5.0	0.25	<0.00885/0.001	0.4490/0.0	7.34	262	2.355	
27, n,a	H_2O	16.8	0	<0.00885	0.4007/0.0100	7.34	262	3.413	
28, a	H_2O	33.9	0	<0.00885	0.4028/0.1148	2.28	262	1.546	
29, a	H_2O/gn.-lhz.	23.9/23.9	0.50	<0.00885/0.001	0.5344/0.1848	3.75	248	1.110	
30, n,a	H_2O/gn.-lhz.	13.8/13.8	0.50	<0.00885/0.001	0.4922/0.2618	7.25	248	2.547	
31, a	H_2O/gn.-lhz.	21.6/28.6	0.57	0.213/0.189	0.3892/0.1469	2.06	248	3.349	0.010
32, a	H_2O	34.6	0	0.247	0.3622/0.0401	2.28	248	2.646	
33, a	H_2O/gn.-lhz.	23.9/23.9	0.50	<0.00885/0.001	0.4865/0.3145	2.28	248	7.541	
34, a	H_2O	35.0	0	<0.00885	0.4249/0.1109	2.28	248	4.481	
35, a	H_2O	35.3	0	<0.00885	0.3802/0.2340	2.28	228	2.178	
36, a	H_2O/gn.-lhz.	24.0/24.0	0.50	<0.00885/0.001	0.4942/0.2996	3.75	228	1.843	
37, a	H_2O	36.2	0	0.227	0.3780/0.1147	2.28	228	1.521	
38, a	H_2O/gn.-lhz.	21.6/28.6	0.57	0.253/0.189	0.3961/0.2357	2.28	228	2.475	0.0035

39, n,a	ammonia ice	<42	0	~0.4	>0.294/?	2.28	77/153	0.18/0.427	
40, a	CO_2	52	0	powder to 0.4 cm	0.4120/0.1421	2.28	77/193	0.20/0.62	
41, a	CO_2	50.4	0	$0.119 < r_i < 0.238$	0.4147/0.1571	2.28	77/192	0.18/0.62	
42, a	ammonia ice	46	0	~0.4	0.3890/0.2146	2.28	77/149	0.27/0.448	
1M	H_2O	34.8	0	0.254	0.3733/0.0	4.43	262	3.191	
2M	H_2O/gn.-lhz.	16.3/41.7	0.72	0.259/0.229	0.4128/0.1183	4.43	262	5.066	0.105
3M	H_2O/gn.-lhz.	16.3/41.7	0.72	0.217/0.155	0.4439/0.1667	4.46	262	12.716	0.126
4M	H_2O/gn.-lhz.	16.3/41.7	0.72	<0.00885/0.001	0.4839/0.1181	4.53	262	14.404	
5M	H_2O	34.8	0	<0.00885	0.4040/0.0	4.48	262	4.924	
6M	H_2O/gn.-lhz.	23.9/23.9	0.50	<0.0175/0.001	0.4423/0.0305	4.58	262	9.207	
7M	H_2O/gn.-lhz.	24.1/24.1	0.50	0.223/0.219	0.4182/0.0762	4.43	262	4.923	0.034
8M	H_2O/gn-lhz.	24.9/24.9	0.50	<0.00885/<0.0175	0.4325/0.1371	4.45	262	0.069	
9M	H_2O/gn.-lhz.	29.7/9.9	0.25	<0.00885/0.001	0.4392/0.0061	4.45	262	11.015	
10M	H_2O/gn.-lhz.	6.5/6.5	0.50	<0.00885/0.001	0.3857/0.0014	17.7	262	7.579	
11M	H_2O/gn.-lhz.	12.0/12.0	0.50	<0.00885/0.001	0.4288/0.0249	9.0	262	4.339	
12M	H_2O/gn.-lhz.	7.13/2.37	0.25	<0.00885/0.001	0.3965/0.0023	17.7	262	3.383	
13M	H_2O/gn.-lhz.	23.7/23.7	0.50	0.224/0.185	0.3993/0.0145	4.51	262	5.939	0.033
14M	H_2O/gn.-lhz.	6.3/6.3	0.50	<0.00885/0.001	0.3987/0.0114	13.3	262	0.628	
15M	H_2O/gn.-lhz.	13.5/4.5	0.25	<0.00885/0.001	0.4207/0.0	9.0	262	3.381	
16M	H_2O/gn.-lhz.	11.5/11.5	0.50	<0.00885/0.001	0.4493/0.0450	8.7	248	2.546	
17M	H_2O/gn.-lhz.	6.15/6.15	0.50	<0.00885/0.001	0.4375/0.0522	17.6	248	1.708	
18M	H_2O/gn.-lhz.	11.6/11.6	0.50	<0.00885/0.001	0.4436/0.0500	7.28	248	3.482	
19M	H_2O/gn.-lhz.	6.05/6.05	0.50	<0.00885/0.001	0.4229/0.0259	13.3	248	0.979	
20M	H_2O/gn.-lhz.	23.7/23.7	0.50	<0.00885/0.001	0.4766/0.1223	4.4	248	7.468	
21M	H_2O	15.3	0	<0.00885	0.3896/0.0086	8.9	248	1.110	
22M	H_2O	34.6	0	<0.00885	0.3849/0.0264	4.38	248	2.432	
23M	H_2O/gn.-lhz.	6.10/6.10	0.50	<0.00885/0.001	0.3965/0.0200	17.3	248	1.534	
24M	H_2O	9.30	0	<0.00885	0.2784/0.0	17.5	248	0.965	
25M	H_2O/snd.	20.0/20.0	0.50	<0.00885/0.001	0.4828/0.671	4.38	248	0.046	
26M	H_2O/met.	11.5/11.5	0.50	<0.00885/0.001	0.4225/0.0547	4.35	248	4.095	
27M	H_2O	9.2	0	<0.00885	0.3139/0.0	13.4	248	0.850	
28M	H_2O/snd.	23.0/23.0	0.50	<0.00885/0.001	0.4533/0.0	4.36	248	1.813	

Comments according to column numbers:

1. In runs #7–#9 and #15–#42 acoustic emissions from compacted samples were recorded; these runs are marked by the the letter "a". The letter "n" denotes that the piston-displacement record is not available.
4. Rock content by mass C_m.
5. Effective radii of ice/rock grains r_i/r_r, or effective radius of ice grains r_i only. For millimeter-size water-ice grains r_i denotes the mean radius of hemispherical grains. For millimeter-size rock grains, r_r denotes their mean size of equivalent spheres. Powder sizes are determined by sieving and verified by microscope.
6. (initial porosity)/(final porosity) $= q_0/q_f$.
9. Recording time.
10. Crushing coefficient κ defined by Equation (9).

In columns 8 and 9, numerators are respectively the lowest temperature of the run and the time interval during which the temperature was stable; denominators are the temperature at the end of the run and the total duration of the run.

Cumulative recording times are

$$\text{Runs } 1 - 42 : \quad \frac{107.4 \times 10^5 \text{ s}}{146.8 \times 10^5 \text{ s}},$$

$$\text{Runs } 1M - 28M : \quad 119.8 \times 10^5 \text{ s},$$

$$\text{70 runs' total} : \quad \frac{227.2 \times 10^5 \text{ s}}{2.66.6 \times 10^5 \text{ s}} = \frac{263.0 \text{ d}}{308.5 \text{ d}}.$$

on an electronic balance with a theoretical accuracy of 0.01 g. However, in practice the accuracy was about five times worse, especially for powder samples that lost mass by evaporation during the few minutes required for mixing the ice and rock powder.

Carbon-dioxide ice grains were produced from a commercial dry-ice block by crushing it. Only two experiments involving samples made from CO_2 (without rock admixture) were conducted. For run 40, the grains were not selected by sieving and therefore all grains below about $r_i = 4$ mm were used; for run 41 the grains were sieved and a size 2.38 mm $< r_i <$ 4.76 mm was selected. CO_2-ice grains were weighed and placed immediately (to avoid considerable loss of mass by sublimation), without counting, into the pressure cylinder previously cooled with liquid nitrogen.

Ammonia-ice grains were prepared by freezing ammonia-water droplets in liquid nitrogen. Ammonia water contains more than 25% and less than 28% of the NH_3. The critical moment in preparing the ammonia-ice sample was when the grains were removed from the liquid nitrogen bath and weighed: the melting point of ammonia ice is about 170 K (for details concerning the ammonia/water system, see Johnson and others (1985), Croft and others (1988) and Kargel and others (1991)). After removing the grains from the bath they soon became soft and started to stick together. To minimize this, the weighed samples were placed as quickly as possible into the pressure cylinder, which had been pre-cooled in liquid nitrogen. The weighing precision was no better than about 2 g (about 4% of the mass of a sample) for runs 14 and 42, and it was even worse for run 39. In such difficult conditions, the ammonia-ice grains were not counted and their size was only roughly estimated.

The lithic component of the samples included garnet-lherzolite, used in 36 experiments, sandstone (three runs) and stony meteorite (only one run; no more material was available).

The garnet-lherzolite came from the Sowie Góry Mountains gneiss block near Bystrzyca Górna in the Polish Sudetes. Its bulk chemical composition in weight per cent is 40.6% SiO_2, 36.5% MgO, 8.9% H_2O, 5.0% FeO, 2.8% Al_2O_3, 2.7% Fe_2O_3, 2.4% CaO, 1.1% others); recalculated on a water-free basis (44.5% SiO_2, 40.0% MgO, 8.2% (FeO)$_{total}$, 3.1% Al_2O_3, 2.6% CaO, 1.6% others); this composition is similar to that of Earth's upper mantle. The approximate mineralogical composition of garnet-lherzolite in volume per cent is: 63% olivine, 17% orthopyroxene, 11% clinopyroxene, 4% garnet, 4% clino-amphibole and 1% spinel. Its density, 3.06 Mg m^{-3}, is close to that commonly assumed for the density of rock components of the bodies belonging to the Outer Solar System.

The sandstone material was collected from a borehole at Kompina, Poland, at a depth interval of 3648–3654 m. The sandstone has a chlorite matrix and its bulk composition by weight is 72% SiO_2, 13.3% Al_2O_3, 3.4% Na_2O, 2% FeO, 1.8% Fe_2O_3 and 7.5% others. Its density is 2.54 Mg m^{-3}. It is weak and easily crumbled.

The meteorite material originates from a 13.81 g fragment of an Antarctic stony meteorite, Ym 74013. This fragment had been used previously in other studies during which it was heated to 1073 K; we assume that the

heating did not significantly affect its mechanical properties. The density of the meteorite is 3.41 Mg m^{-3}; chemical and mineralogical analyses have not been conducted.

The rocky material was crushed and sieved. For the samples prepared from rock grains millimeters in size, the grains were weighed and counted. The mean radii of the rock grains (Table 2) are calculated assuming they are spherical in shape.

The rock component can play a "passive" or an "active" role in the compaction of ice/rock mixtures. We define the passive behavior as that when the rock grains do not crush and hence when the pores do not fill with the smaller rock fragments. In such a case, the volume of pores diminishes only because of crushing and creep of ice grains. The rock grains play the role of rigid inclusions affecting the re-arrangement and deformation of the ice grains. Rock grains play an active role when they crush. In the following, we define the crushing coefficient κ. The counting and weighing of rock grains performed before a run were repeated after the run: after thawing, the recovered sample was dried and the same number of the largest recovered rock grains as the number of rock grains n_r initially comprising the sample was weighed. We define the crushing coefficient as

$$\kappa = 1 - \frac{\text{recovered mass of the largest } n_r \text{ rocky grains}}{\text{initial mass of all } n_r \text{ rocky grains}}.$$

(9)

When $\kappa = 0$, the rock grains initially in the sample were not crushed at all. On the other hand, when $\kappa \to 1$ the rock grains were almost completely crushed to powder during compaction. One can expect that the crushing coefficient, for fixed rock, increases when pressure and/or rock concentration increases. For fixed pressure and concentration, κ is expected to be greater for weaker rocks. The results listed in Table 2 support this speculation: κ is generally around 0.02 for H_2O/gn.-lhz. samples, which is distinctly lower than for H_2O/snd. samples ($\kappa \cong 0.2$).

3. EXPERIMENTS

The primary output from the experiments is the change in porosity as a function of time generally under fixed stress and temperature conditions. In addition, interesting results were obtained from records of strain versus time for fixed stresses and variable temperatures.

Records of acoustic emission (number of single acoustic events above a certain threshold recorded in a time interval versus time) and the microscopic photography of thin sections of the recovered samples (for samples prepared from powdered material) provide supplementary information on the compaction processes.

Two types of apparatus were used.

3.1. Apparatus in which pressure is produced by loading of a sample by mechanical weights

This is a modified version of equipment used in the experiments of Ebinuma and Maeno (1985, 1987) and Ebinuma (1987). Three brass and stainless-steel piston–

cylinder systems were applied, with inner radii of 1.5 and 1.06 cm (cross-sections of 7.06 and 3.53 cm^2), respectively. The cylinder height is 13 cm and the maximum initial height of a sample was $\cong 12$ cm. However, in most of the runs (CO_2 and ammonia samples being the exceptions), the initial height and volume of the samples were about 8.5 cm and 60 cm^3; the initial aspect ratio (diameter/height) was about 0.35; the final value was up to about 0.6. If the aspect ratio is too small, as it is in the thinner cylinder, the friction between a compacted sample and the wall of the cylinder influences the experimental results considerably. For that reason, the piston displacements for some runs cannot be taken into account.

The pressure was applied by placing steel weights on the piston, therefore the pressure increases incrementally during the loading phase.

The runs at 262, 248 and 228 K were conducted under cold-room temperature conditions, and all elements of the equipment were at the same temperature.

During the runs with temperatures of the cooling medium equal to 195 K (solid CO_2 mixed with ethanol) and 77 K (liquid N_2), maintenance of stable temperatures was difficult due to heat conduction. The temperature was monitored by three copper/copper–nickel thermocouples mounted 0.3 cm below the bottom of the sample, on the wall of the cylinder 3 cm above the bottom and within the piston 0.3 cm above the sample top (Fig. 1).
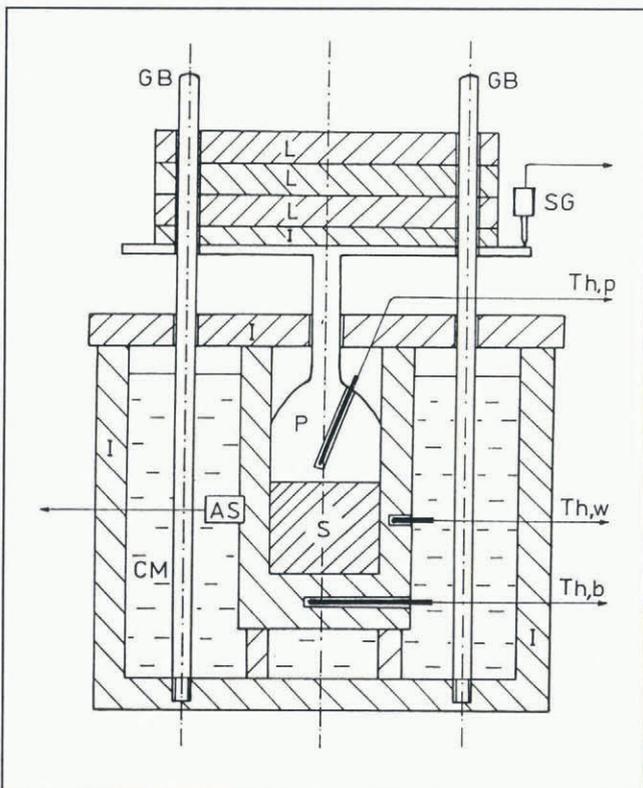

Fig. 1. Schematic diagram of the apparatus in which pressure is produced by loading a sample with weights. S, sample; P, piston; L, loads; GB, guide bars for loads; SG, strain gauge; AS, acoustic-emission sensor; Th, thermocouples mounted in the bottom of cylinder (b), inside of its wall (w) and inside of the piston (p); CM, cooling medium (if any); I, thermal insulator.

The average of three temperatures was taken to be the sample temperature. The difference of temperature from the bottom to the top of the sample was about 10 K during stable cooling conditions, or even more during a period just after evaporation of the cooling medium. Thus, the temperature regime varied from stable and cold (while in the cooling bath) through variable to constant (while in the cold room). Measurements of piston displacements were difficult in the cooling bath. Much more accurate results could be obtained when the temperature increased above a certain threshold, at which point the piston-displacement rate and the acoustic emission activity increased considerably. This was the motivation for conducting the experiments in the variable temperature regime.

An acoustic-emission transducer was mounted on the lateral wall of the cylinder. In this work, the details of acoustic emission activity are not considered; however, it is worth mentioning that peaks in activity were correlated with rapid consolidation. This suggests that consolidation is caused by continuous deformation of material interrupted by abrupt cracking events.

3.2. Apparatus with oil press

This equipment allows us to reach higher pressures than with the previous apparatus, but it is restricted to temperatures above 248 K, since no cooling medium can be applied. Pressure was increased smoothly (not step-like) to maximum pressures of 4.4, 9.0, 13.3 and 17.7 MPa. The higher pressure requires the piston–cylinder system to have a smaller cross-section. Three different stainless-steel piston–cylinder systems were used with cross-sections of 12.56, 6.246 and 3.173 cm^2. The corresponding initial volumes of the samples were about 60, 30 and 15 cm^3; the initial ratio of sample diameter to sample height was about 0.84; the final ratio was up to about 1.5. The cold-room temperature was 262 and 248 K. Pressure and temperature were continuously recorded. Pressure was stable within an interval of $\pm 1.5\%$ or better, and temperature variability was ± 1 K. The sample-mounting system inside the oil-press apparatus does not permit recording acoustic emission from the sample.

3.3. Piston-displacement recording

The experimental accuracy of the displacement measurement in all runs was about 0.1 mm. For the low-temperature runs when the cooling medium was used, as well as for the final periods of strain monitoring for the runs performed in typical cold-room temperatures, the piston displacement is very small, just on the limit of accuracy. Therefore, for low-temperature runs, an estimate of the upper limit of compaction rate requires stable temperature conditions to be maintained at least for a few hours. The final stage of a typical cold-room run requires more than a 1 d period for reliable measurements of compaction rate.

The piston–cylinder method used in our experiments is complicated by friction between the sample and the cylinder, which inhibits sample compaction. The flatter the sample is, the smaller the friction effects are. However,

flatter samples were not used because piston displacement for such samples would be so small as to render accurate measurement of porosity changes difficult. A loose fit between the piston and the cylinder's walls is important, otherwise the piston readily freezes to the cylinder. No rings or seals were necessary. It is difficult to estimate reliably the magnitude of friction effects; they are neglected in the analysis of the results.

Another potential complication that can affect the experiments is the pressure of air trapped within the samples. A simple calculation shows that the air pressure in the pores is not important when compared with external pressure. Indeed, consider the porosity $q_p = 0.1$ to be at the limit for air percolation and the porosity $q_m = 0.02$ to be the lower limit of reliable porosity measurements. The pressure of air trapped in pores (when $q_p \leq q \leq q_m$) is no higher than $q_p/q_m = 5$ times the atmospheric pressure, which is much less than the external pressure used in the experiments.

4. RESULTS

4.1. General approach

Experimental records of piston displacement versus time t permit the evaluation of the compaction rate $-\dot{q}$ as a function of the porosity q. For each run, we first sought simple expressions between q and $\log t$, or $\log(-\dot{q})$ and $\log t$. Finally, an equation of the form

$$\log(-\dot{q}) = f(q, \log q; \, p, T, C_v) \tag{10}$$

was fitted to a complex of experimental results. The numerical coefficients in Equation (10) depend on sample-specific material parameters.

In the experiments, time is measured from the moment $t = 0$, when the sample is first loaded. An initial period of each experiment t_0, some 50–600 s, was used for the increase of pressure until it reached a required value; $q(t_0) \equiv q_0$. Piston displacements and hence q tend to decrease continuously with time during the initial period (runs #1M–#28M and most of the other runs performed at a temperature not lower than 248 K; Fig. 2a). Displacements are often discontinuous for low-temperature runs (step-like; Fig. 2b). Once a stable pressure is established, the porosity decreases continuously for runs with $T \geq 248$ K. For lower temperatures, the consolidation is generally but not invariably continuous.

Let us discuss the runs with the characteristically continuous consolidation. For the majority of experiments, large segments of the data can be approximated by:

$$\log(-\dot{q}) = A - B \log t. \tag{11}$$

Correlation coefficients obtained by standard linear-regression analysis are frequently as high as 0.99 or even 0.999 for porosity changes as great as $\cong 0.2$, which is half of the whole range of porosities in the experiments. In our preliminary study of experimental results (Leliwa-Kopystyński and others, 1990), the coefficient B in Equation (11) was narrowly defined: $B \simeq 1.7$ for 262 K, and it decreases to $B \simeq 1.2$ for 203 K.

In fitting the data with

$$\log(-\dot{q}) = A + Bq, \quad B > 0, \tag{12}$$

the coefficient B varied from run to run with a large range of approximately 10 to 100. At a first glance, there is no correlation between the values of B and the parameters p and C_v. However, B is clearly greater when (i) the temperature of a run is relatively low or, when (ii) the sample is highly compacted. This second feature prompted us to analyze our data.

To ensure that the compaction rate $-\dot{q}$ vanishes as the porosity q approached zero, we fitted the following expression

$$-\dot{q} = 10^{A+Bq}q. \tag{13}$$

This is a particular case of Equation (10), with which the rate at which porosity decreases is proportional to the porosity. This proportionality corresponds to power-law creep written in a form valid for low porosity $q < 0.1$ (Eluszkiewicz, 1990; after Ashby, 1988). Ashby distinguished six main densification mechanisms for granular materials: pressure-driven volume diffusion, pressure-driven boundary diffusion, surface-tension driven boundary diffusion, Nabarro–Herring creep and power-law creep. Rates of pressure-driven volume diffusion and power-law creep are particularly dependent on porosity. In both mechanisms, the compaction rate depends on temperature, mostly through a similar $\exp(-Q/RT)$ term where Q is the activation energy for a given mechanism and $R = 8.314 \, \mathrm{J \, mol^{-1} \, K^{-1}}$. Only the power-law creep depends strongly on actual pressure; for details concerning densification mechanisms of porous media see Elusuzkiewicz (1990), after Ashby (1988) (general) and after Kirby and others (1987) (water ice). Anticipating results discussed later, we can consider power-law creep to be the main mechanism for compaction of the granular ice/rock mixtures under constant-pressure conditions. If pressure does not remain constant (as during the initial
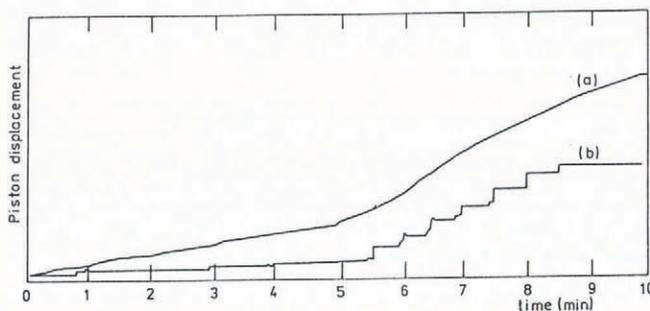

Fig. 2. Piston displacement versus time records. $H_2O/$ garnet-lherzolite samples with $C_m = 0.57$ and thus $C_v = 0.285$. (a) Run #8 with $T = 262$ K; $r_i/r_r = 0.292 \, cm/0.249 \, cm$; continuous displacements. (b) Run #13 with $T < 133$ K; $r_i/r_r = 0.212 \, cm/0.191 \, cm$; jerky displacements. In both runs until $t = 0$ s, the sample was initially loaded by the piston weight only. Next, at $t = 0$, 60, 120, 180 and 240 s, pressure was increased each time by 0.088 MPa, and from $t = 300$ s until $t = 510$ s it was increased by 0.223 MPa every 30 s. Piston displacements are given in arbitrary units.

phase of laboratory experiments or during the formation epoch of the satellites when previously accreted ice/rock regolith layers are loaded by later deposits) substantial densification also occurs by crushing and re-arrangement of grains. In this case, since the rock grains are considerably stronger than the ice, they play an important role in the re-arrangement and creep of ice. Such a situation corresponds to low values of the crushing coefficient $\kappa < 0.02$, Equation (9), and is certainly valid for H_2O/gn.-lhz. samples with $C_m \leq 0.5$ studied under pressure up to 4.5 MPa (Table 2).

Bearing in mind the power-like dependence of compaction rate on pressure and its exponential dependence on temperature, one can postulate the simplest form of the parameters A and B in Equation (13):

$$A = \alpha_0 + \beta_0 \log p - [\delta_0 - \delta \log(1 - C_v)]/T \quad (14)$$

$$B = \alpha + \beta \log p. \quad (15)$$

Thus, Equation (13) takes the following form

$$-\dot{q} = q 10^{\alpha_0 + \alpha q} p^{\beta_0 + \beta q} \exp\left[-\frac{\delta_0 - \delta \log(1 - C_v)}{\log e}\frac{1}{T}\right]. \quad (16)$$

For a given sample (C_v = const), under fixed pressure and temperature, A and B can be found by linear regression applied to Equation (13) having taken the logarithm of both sides. An analysis of sufficient runs provided the values of coefficients $\alpha_0, \cdots, \delta$ (Table 3).

Parameter δ_0, Equation (14), is related to the activation energy Q for power-law creep of pure ice: $\delta_0/(T \log e) = Q/(RT)$. Hence,

$$\delta_0 = 52.24Q \quad (17)$$

where δ_0 is in degrees Kelvin and Q is in kJ mol^{-1}. The activation energy E of the ice/rock mixture is

$$\delta_0 - \delta \log(1 - C_v) = \frac{E}{R}\log e, \quad E = Q + \Delta \quad (18)$$

Table 3. Empirical coefficient in Equation (16) obtained by regression analysis on data from 28 runs with H_2O/garnet-lherzolite powder samples

Parameter	Range of porosity			Other studies
	0.08–0.02	0.16–0.11	$\cong$0.38–0.02 full available range of q	
α_0	4.8	10.5	8.3 $\pm$ 18.4[*]	11.8 $\pm$ 0.4 (1)
β_0	3.3	5.1 $\pm$ 0.5	6.1 $\pm$ 1.1	4.0 $\pm$ 0.6 (1) 3 (2)
δ_0, 10^3 K	3.2	4.9	4.5 $\pm$ 4.8[*]	
α	10.4	10.7	11.7 $\pm$ 1.1	
β	9.0	8.2	6.5 $\pm$ 1.6	
δ, 10^3 K	3.2 $\pm$ 0.3	4.8 $\pm$ 1.2	6.0 $\pm$ 2.5	
$Q_0 = \delta_0/52.24$ kJ mol^{-1}	61.7	94.2	86.9 $\pm$ 91.5[*]	91 $\pm$ 2 (1)

[*] However, the term $(\alpha_0 - \delta_0/T)$ for $T = 262$ and 248 K was found, with reasonable error bar, to be:

$\alpha_0 - \delta_0/262$	9.03 $\pm$ 0.35
$\alpha_0 - \delta_0/248$	10.01 $\pm$ 0.97

(1) Kirby and others (1987) for 240–258 K.
(2) Smoluchowski and McWilliam (1984).

where the term Δ reflects the presence of rock grains. The term $\log(1 - C_v)$, but not C_v itself, is introduced in Equation (14) to ensure that the compressibility of the ice/rock medium vanishes as the amount of ice approaches zero ($C_v \to 1$). In this case, according to Equation (18), the effective excess activation energy Δ should go to infinity, in accordance with the observation that the pressures applied in our experiments were insufficient to induce creep in the rock grains.

4.2. H_2O/rock powder mixtures at 262–228 K

Twenty-eight runs were completed using powdered water ice and garnet-lherzolite with two initial grain-sizes: $r_i < 0.0885$ mm and $r_r \cong 0.01$ mm. The pressure ranged from 2.28 to 17.7 MPa. The garnet-lherzolite concentrations by volume were 0, 0.0909, 0.231 and 0.434 (one run only), and the temperatures were 262, 248 and 228 K (two runs only). For different runs, Equation (16) was fitted within a series of porosity intervals, all being within the 0.38–0.02 porosity range. In addition, regression analyses were conducted for two particular porosity intervals: $q \cong 0.08$–0.02 and 0.16–0.11 (Table 3). Focusing on a particular porosity interval is physically reasonable since the dominant pore-closure mechanism can vary over a broad porosity range. On the other hand, any particular choice of porosity interval diminishes the number of runs available for analysis. Including larger ranges of q in the regression analysis provides more comprehensive relations but may result in lower accuracy. Nevertheless, a "universal" equation, covering the large range of porosity and other parameters, would be very useful in modeling the internal structure and evolution of the icy satellites.

The results in Table 3 require a few remarks. (1) The error bars for coefficient values are marked for the entire range of porosity available; the number of runs is insufficient to assess errors reliably. (2) The coefficients α_0 and δ_0 for the entire range of porosity are very poorly constrained. However, quite reasonable estimates were obtained for the combination $(\alpha_0 - \delta_0/T)$ for temperature ranging from 262 K to 248 K. This arises from the $10^{\alpha_0 - \delta_0/T}$ term in Equation (16), which permits the $(\alpha_0 - \delta_0/T)$ combination to be estimated more accurately than either α_0 or δ_0 taken independently. (3) The results from other researchers for the creep of water ice also follow the power law $10^{\alpha_0} p^{\beta_0} \exp(-Q/RT)$. Apart from reporting results for 240–258 K, which are comparable to ours, Kirby and others (1987) presented results from two other temprature ranges. They found that α_0, β_0 and Q for $T = 195$–240 K are 5.10 ± 0.03, 4.0 ± 0.1 and $61 \pm 2 \text{ kJ mol}^{-1}$, respectively; for $T \leq 195$ K, they are -2.8 ± 0.6, 4.7 ± 0.3 and $36 \pm 5 \text{ kJ mol}^{-1}$, respectively.

In Figure 3a–d representative experimental curves of compaction rate versus porosity are compared with the regression (Equation (16)) obtained from all data. Particular parameters were: $\alpha_0 = 8.29$, $\beta_0 = 6.1$, $\delta_0 = 4539$ K, $\beta = 8$ and $\delta = 4500$ K. For runs at 262 K, the coefficient α was set to 11.7. As the slopes of the compaction-rate curves increase strongly with decreasing temperature (Fig. 3d), it was useful to introduce a linear relation between α and the reduced

temperature, $T_{\text{melting}} - T$. For the samples containing water ice,

$$\alpha = 9.5 + a(273 - T), \qquad (19)$$

preliminary estimates of a being 0.2. Experiments over a larger interval of temperature are needed to determine a more accurately.

The dominant role of temperature in the rheological Equation (16) is expressed through the exponential term. The term $10^{\alpha q}$ in which α varies with temperature (Equation (19)) is less important; moreover, its role diminishes with decreasing porosity.

Experimental results for pure H_2O powders and H_2O/rock powders for three different rocks are presented in Figure 4. The rock content by mass was $C_m = 0.5$ and, hence, the volume concentrations C_v were 0.212, 0.231 and 0.265 for an Antarctic meteorite, garnet-lherzolite and sandstone, respectively. The dashed lines represent fits, Equations (16) and (19), to the experiments. The fit is adequate for the H_2O and H_2O/gn.-lhz. samples, as expected since these samples were used for developing the fitting formulae, and it is also adequate for the H_2O/met. sample. However, the fit fails for the H_2O/snd. sample, presumably because sandstone is a soft rock; its crushing coefficient κ (Equation (9); Table 2) is an order of magnitude greater than that of garnet-lherzolite. Sandstone may play the role of "a lubricant" with water ice. In Equation (16), only the coefficient δ reflects a lithological influence on the rheological behaviour; thus, one can conclude that $\delta_{\text{snd.}} < \delta_{\text{gn.-lhz.}}$. The experiment with rock of a meteoric origin (run # 26M; Fig. 4) gives a rheological effect similar to that for the garnet-lherzolite admixture. This similarity provides yet another argument (beside the mineralogical and cosmochemical ones) that garnet-lherzolite is a more realistic material than sandstone for examining the ice–rock rheology in the Solar System.

4.3. H_2O and H_2O/garnet-lherzolite mm-sized mixtures at 262–140 K

Results from the two series of experiments are presented in Figures 5 and 6. We were not able to fit a formula of the type of Equation (16) due to the scarcity of data. However, two very important conclusions can be drawn from the results. First, garnet-lherzolite in water ice ($C_v = 0.231$) reduces the rate of pore closure by at least two orders of magnitude. Secondly, no influence of grain-size on compaction rate was observed.

4.4. CO_2 ice and ammonia ice

Only five runs, at 2.28 MPa, were made with these materials: two with CO_2 ice and three with ammonia-water ice (about 25% NH_3). However, these preliminary experiments allowed the activation energy Q to be estimated. A formula fitted to the experiments was

$$-\dot{q} \propto q \exp\left(-\frac{\delta_0}{\log e}\frac{1}{T}\right) \qquad (20)$$

and thus similar to Equation (16); the coefficient δ_0 has the same meaning as previously (Equation (17)). It was
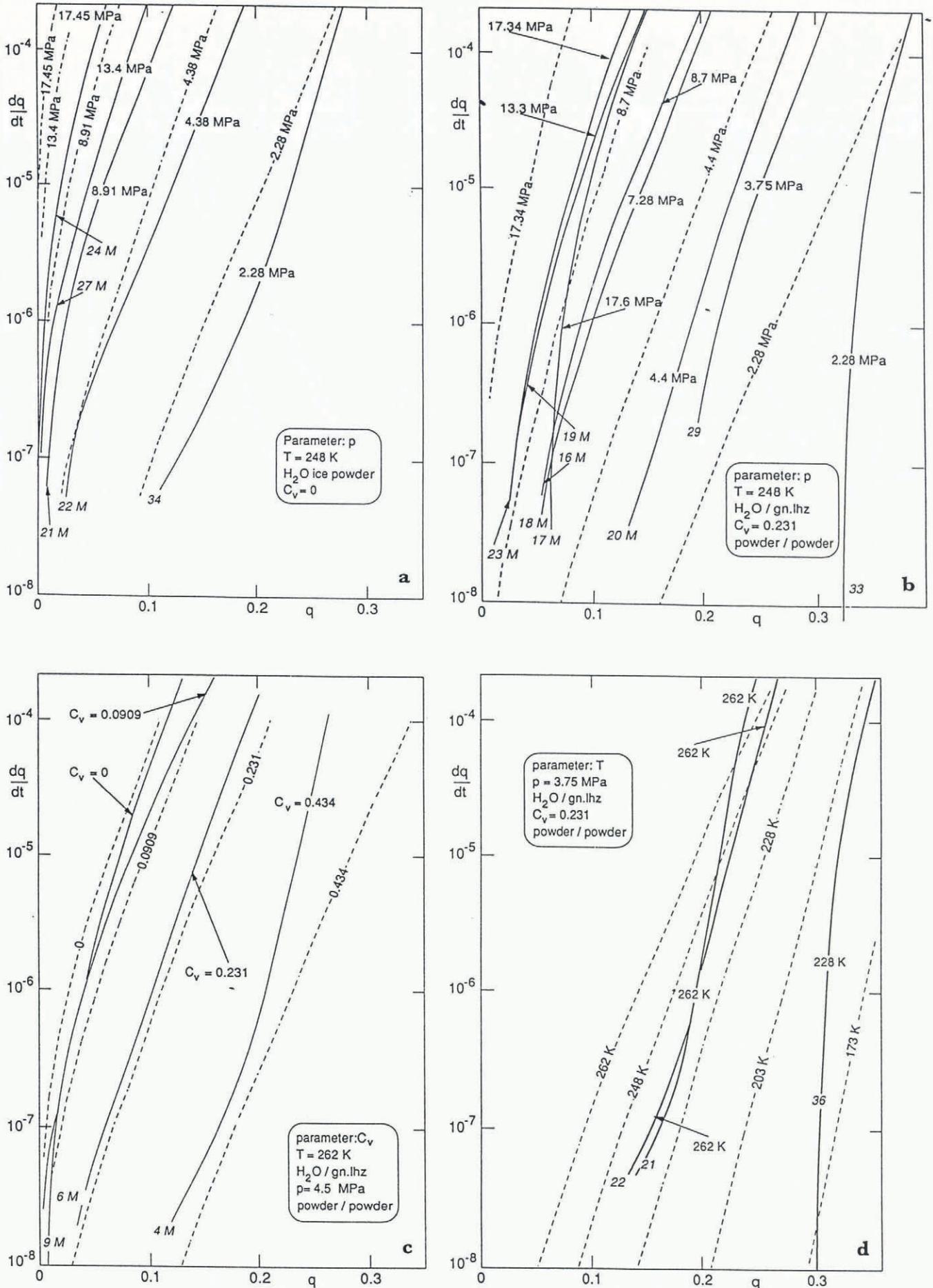
Fig. 3a–d. Compaction rate versus porosity. Solid lines: experiments; the label for each run allows reference to Table 2 for additional information. Dashed lines: curves fitted to experiments by means of Equation (16), with appropriate parameters p, T, C_v and coefficients α, ..., δ, which were found for H_2O/gn.-lhz. powder/powder mixtures for the entire porosity range examined (see Table 3).
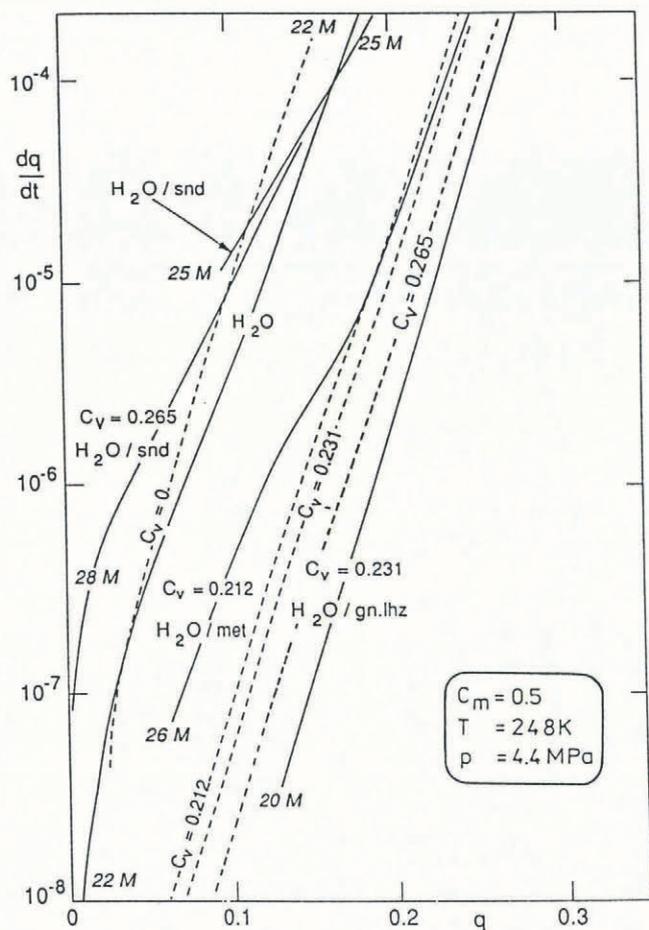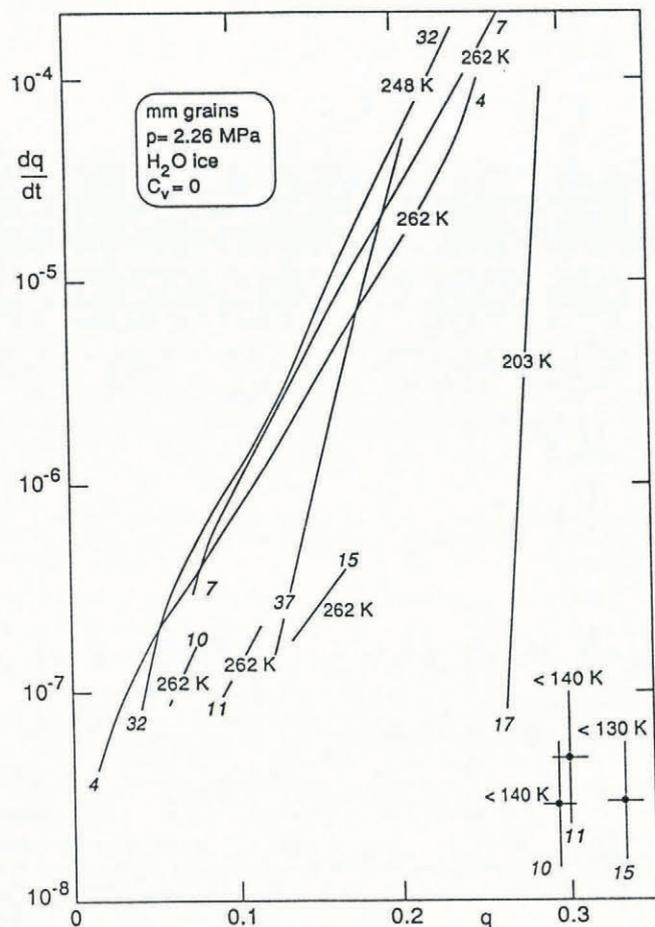
Fig. 4. See caption for Figure 3a–d.

Fig. 5. Compaction rate versus porosity for different temperatures. Experiments with H_2O samples prepared from mm-sized grains.

estimated that for CO_2 ice between 105 K and 190 K δ_0 is about 400 K, corresponding to an activation energy Q of about 10^4 J mol^{-1}. For ammonia ice under similar pressure and within the 100–120 K temperature interval, $\delta_0 \cong 1000$ K and therefore $Q \cong 2.5 \times 10^4$ J mol^{-1}. More experiments are required to substantiate these results and to assess the pressure-dependence of the coefficients.

5. CONCLUSIONS

The presence of rock fragments ($\cong 25\%$ by volume) in porous H_2O ice can decrease its compaction rate by about two orders of magnitude (for pressures ≤ 17.7 MPa and temperatures 228–262 K). This inhibitory effect is likely to be even more pronounced at lower temperatures and high porosities $q \cong 0.3$ but additional studies are necessary to substantiate this (Figs 5 and 6).

The rheology of the CO_2 and ammonia ices was studied here apparently for the first time. Preliminary results show that these materials are more easily compacted than H_2O ice. As expected, their rheological behaviour is dictated by pressure, temperature and porosity. The activation energies of H_2O, CO_2 and ammonia ices were measured.

Our results have direct implications for studies of the evolution of satellites and may also pertain to aspects of glaciers on Earth.
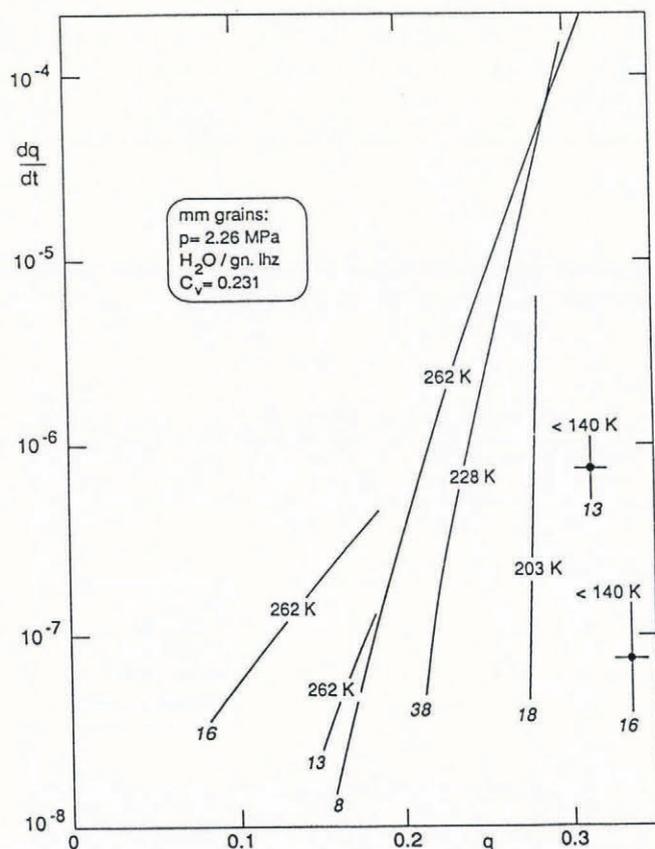

Fig. 6. Compaction rate versus porosity for different temperatures. Experiments with H_2O/garnet-lherzolite samples prepared from mm-sized grains.

ACKNOWLEDGEMENTS

REFERENCES

Ashby, M. F. 1988. *Background reading: hot isostatic pressing and sintering.* Cambridge, University of Cambridge. Engineering Department.

Croft, S. K., J. I. Lunine and J. Kargel. 1988. Equation of state of ammonia-water liquid: derivation and planetological applications. *Icarus*, **73**, 279–293.

Ebinuma, T. 1987. Studies on the pressure-sintering of ice and the densification mechanism of snow. (Thesis, Hokkaido University at Sapporo. Institute of Low Temperature Science.)

Ebinuma, T. and N. Maeno. 1985. Experimental studies on densification and pressure-sintering of ice. *Ann. Glaciol.*, **6**, 83–86.

Ebinuma, T. and N. Maeno. 1987. Particle rearrangement and dislocation creep in a snow-densification process. *J. Phys.* (Paris), **48**, *Colloq.* C1, 263–269. (Supplément au 3.)

Ellsworth, K. and G. Schubert. 1983. Saturn's icy satellites: thermal and structural models. *Icarus*, **54**(3), 490–510.

Eluszkiewicz, J. 1990. Compaction and internal structure of Mimas. *Icarus*, **84**, 215–225.

Eluszkiewicz, J. and J. Leliwa-Kopystyński. 1988. A model of the porous structure of icy satellites. *In Proceedings of the Eighteenth Lunar and Planetary Conference*. Cambridge, Cambridge University Press, 741–747.

Eluszkiewicz, J. and J. Leliwa-Kopystyński. 1989. Compression effects in rock-ice porous mixtures: an application to the study of satellites. *Phys. Earth Planet. Inter.*, **55**(3–4), 387–398.

Johnson, M. L., A. Schwake and M. Nicol. 1985. Partial phase diagram for the system NH_3–H_2O: the water-rich region. *In* Klinger, J., D. Benest, A. Dollfus and R. Smoluchowski, *eds. Ices in the solar system.* Dordrecht, etc., D. Reidel Publishing Co., 39–47. (NATO ASI Series C 156.)

Kargel, J. S., S. K. Croft, J. I. Lunine and J. S. Lewis. 1991. Rheological properties of ammonia-water liquids and crystal-liquid slurries: planetological applications. *Icarus*, **89**, 93–112.

Kirby, S. H., W. B. Durham, M. L. Beeman, H. C. Heard and M. A. Daley. 1987. Inelastic properties of ice I_h at low temperatures and high pressures. *J. Phys.* (Paris), **48**, *Colloq.* C1, 227–232. (Supplément au 3.)

Leliwa-Kopystyński, J., S. Murakami, Y. Mizuno, N. Maeno and N. Bakun-Czubarow. 1990. Compaction of icy/rocky porous mixtures at low temperatures (from 262 K to 77 K) — preliminary results. *High Pressure Research*, **5**, 696–698.

Lewis, J. S. and R. G. Prinn. 1984. *Planets and their atmospheres.* London, Academic Press.

Smoluchowski, R. and A. McWilliam. 1984. Structure of ices on satellites. *Icarus*, **58**(2), 282–287.

Smoluchowski, R., M. Marie and A. McWilliam. 1984. Evolution of density in solar system ices. *Earth, Moon and Planets*, **30**, 281–288.

Squyres, S. W., R. T. Reynolds, A. L. Summers and F. Shung. 1988. Accretional heating of the satellites of Saturn and Uranus. *J. Geophys. Res.*, **93**(B8), 8779–8794.

Thomas, P. C. 1988. Radii, shapes, and topography of the satellites of Uranus from the limb coordinates. *Icarus*, **73**, 427–441.

The accuracy of references in the text and in this list is the responsibility of the authors, to whom queries should be addressed.